

DESIGN AND INVESTIGATION OF A SHORT-TO-MEDIUM-RANGE AIRCRAFT WITH LIQUID HYDROGEN AND SAF MULTI-FUEL PROPULSION

Barlas Türkyilmaz[1], Moritz G. Kolb[1], Xin Zhao[2] & Mirko Hornung[1]

[1]Bauhaus Luftfahrt e.V., Willy-Messerschmitt-Str. 1, 82024 Taufkirchen, Germany
[2]Chalmers University of Technology, 412 96 Gothenburg, Sweden

Abstract

In this paper, a multi-fuel (SAF and liquid hydrogen) short-to-medium-range aircraft is designed and evaluated against a kerosene/SAF only baseline aircraft. The study setup and methodology are explained, including the design and fuel utilization strategy for the multi-fuel aircraft. A more efficient liquid hydrogen tank integration in the aft fuselage, facilitated by the utilization of a T-tail instead of a conventional tail, reduces the energy penalty of the multi-fuel aircraft from 8.9% to 4.6%. Although the multi-fuel aircraft consumes more energy than the baseline aircraft, it can be advantageous by up to 27% in 2050 in terms of energy costs tied to aircraft operation.

Keywords: BLADE, short-to-medium-range aircraft, multi-fuel propulsion, overall aircraft design, HOPE

1. Introduction

The aviation sector is expected to grow to 2.7 times its current size in terms of number of passengers travelling annually by 2050 [1], which will lead to a significant increase in the climate footprint of the sector without mitigating action. Therefore, the contribution of aviation to global warming, which was estimated as 3.5% up to 2018 [2], can be expected to increase. Hydrogen is being considered more often in recent studies as an alternative energy carrier in aviation, but its storage in aircraft is connected to significant penalties due to its cryogenic storage conditions, which are fulfilled with near-cylindrical fuselage tanks, and therefore the necessitated increase in fuselage volume. A multi-fuel aircraft, powered by liquid hydrogen (LH_2) and sustainable aviation fuel (SAF), would be able to cover a significant portion of the short-to-medium-range (SMR) market while flying with LH_2 only, but with smaller performance penalties compared to a LH_2 aircraft which is designed to fly the entire design range with LH_2. This would allow airlines to retain the operational flexibility of a conventional SAF aircraft, which can also utilize fossil kerosene or any SAF mix with higher availability and fly longer ranges with less penalties, while also benefiting from LH_2 as an alternative energy carrier. Even though previous research has considered LH_2-kerosene/SAF multi-fuel aircraft before, these aircraft are either retrofit studies of current airframes flying or in development [3–5], or use only one type of energy carrier during the sizing mission [6]. The HOPE (**H**ydrogen **O**ptimized multi-fuel **P**ropulsion system for clean and sil**E**nt aircraft) project [7], which is co-funded by the European Union's Horizon 2022 program and UK Research and Innovation, is investigating the clean-sheet design of a multi-fuel SMR aircraft. It consists of a conventional tube-and-wing configuration, a single LH_2 tank positioned in the aft fuselage, multi-fuel-burning turbofans under the wing, complemented with a boundary-layer-ingesting (BLI) fan powered by a fuel-cell auxiliary propulsion and power unit (FC-APPU). This aircraft is derived in a stepwise manner by first defining a baseline aircraft [8], then deriving a multi-fuel aircraft with a fuel-cell auxiliary power unit (FC-APU) from the baseline, which is used to derive the multi-fuel aircraft with the BLI fan and FC-APPU. This paper focuses on the design of a multi-fuel aircraft without the BLI fan, with emphasis on the effects of the multi-fuel propulsion on the overall aircraft level, the design choices and sizing strategy. This multi-fuel aircraft is compared to the conventional kerosene/SAF-fueled baseline aircraft, which is sized to the same top-level aircraft requirements (TLARs), to evaluate the performance of the multi-fuel aircraft.

https://doi.org/10.71945/icas2026_0073

2. Methodology

This chapter gives an overview of the methodology used for the aircraft design study in this paper. The TLARs for the aircraft class considered are presented first. Afterward, the derivation process for the multi-fuel aircraft is explained in general. The multi-fuel propulsion system is introduced next, with specific sections related to the multi-fuel burning turbofans and the FC-APU system. The aircraft sizing strategy, such as the logic on how the LH_2 is used for each mission and how the amount of LH_2 for the design of the tank is determined, are explained in the final section of this chapter.

2.1 Top-Level Aircraft Requirements

To assess the performance of the multi-fuel aircraft, it is compared to a conventional kerosene/SAF powered baseline aircraft with the same technology level, which is referred to as the HOPE-BL [8]. All aircraft shown in this paper are sized to the same TLARs and using the same technology assumptions for an entry-into-service (EIS) in 2035. An excerpt of the TLARs can be found in Table 1. Regarding the representative technology factors used in sizing the aircraft for an EIS in 2035, the reader is referred to [8].

Table 1: Aircraft TLARs [8]

Parameter	Value
EIS	2035
Design range	3000 nmi (US trans-continental)
Design number of passengers (single-class)	180
Design payload	18000 kg
Max. payload	19260 kg
Max. operating Mach	0.82
Initial cruise altitude	≥ FL330
One-engine out ceiling	FL170
TOFL (MTOM, ISA, SL)	≤ 2000 m
LFL (MLM, ISA, SL)	≤ 1900 m
Time-to-climb	≤ 25 min
Airport compatibility	ICAO Code C Wingspan <36 m V_{ref} ≤ 140 KCAS

Additional to these TLARs, the reserves are calculated using a 200 nautical mile (nmi) diversion, 30 minutes of holding and 3% of trip fuel as final reserve. The design mission is flown at with a deviation of +10 K to the International Standard Atmosphere (ISA) conditions to allow for a certain excess engine performance in ISA conditions during the sizing process. The typical mission, however, is flown under ISA conditions. The climb is performed with a speed of 250 KCAS below FL100, 300 KCAS above FL100 until the crossover altitude where a Mach number of 0.78 is reached, which is maintained until the end of the climb. The same schedule is kept for the descent.

In contrast to the HOPE-BL, the typical mission range is increased to 1000 nmi, as this value is used to size the LH_2 tank for the multi-fuel aircraft. Further information regarding the reasoning behind this value is provided in Section 2.4.

2.2 Aircraft Derivation

As previously mentioned in Chapter 1, this study is undertaken using a stepwise approach. The starting point and the comparison baseline is the HOPE-BL, which is converted to utilize the multi-fuel propulsion system. This involves the replacement of the conventional baseline engine with the multi-fuel burning turbofans, as well as the substitution of the conventional auxiliary power unit (APU) with the FC-APU. Additionally, the LH_2 tank and fuel system are added to facilitate the storage and distribution of the second energy carrier. Using the sizing strategy described in Section 2.4, this aircraft is sized to meet all TLARs, which results in the HOPE-MF aircraft.

While conducting the design space exploration studies for HOPE-MF, it became clear that the LH_2 tank integration is pivotal to the resulting aircraft performance. HOPE-MF has a conventional tail layout, which restricts the tank end position inside the fuselage regarding space constraints for the horizontal tailplane (HTP), which requires space for the jackscrew among other related systems. To gain design freedom with the tank end position, an additional multi-fuel aircraft is investigated, which is sized to the

same TLARs and has the same engine, fuel system and tank models, but features a T-tail configuration. This enables the LH_2 tank to move further aft in the fuselage, allowing a shorter fuselage length. This aircraft is referred to as the HOPE-MF-TT. A schematic of the aircraft derivation process is illustrated in Figure 1.

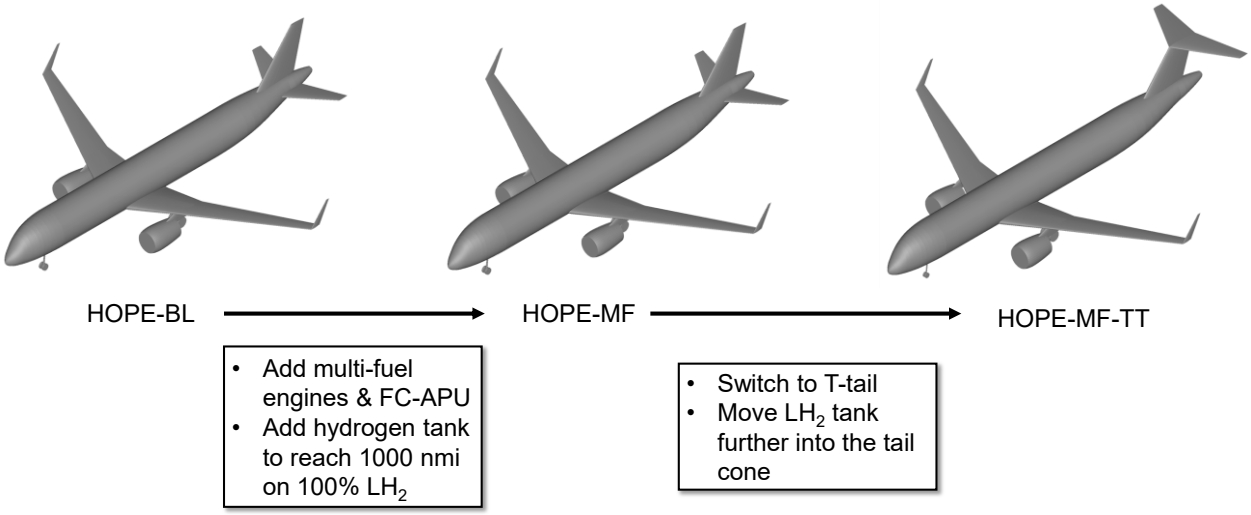


Figure 1: Aircraft derivation process

2.3 Multi-Fuel Propulsion System and Aircraft Subsystems

The multi-fuel aircraft for the HOPE project is powered by two under-wing mounted ultra-high bypass ratio (UHBR) geared turbofan (GTF) engines featuring a multi-fuel combustion chamber capable of burning pure SAF, pure LH_2 or a mixture of both fuels. Furthermore, the aircraft is equipped with an FC-APU, which provides electrical power to all aircraft subsystems throughout the entire mission envelope. The following sections provide an overview of the implemented modelling methods, system architectures and sizing logic implemented for the under-wing engines and FC-APU system.

2.3.1 Multi-Fuel Ultra-High Bypass Ratio Turbofan Engines

The under-wing multi-fuel UHBR GTF power plants represent a key enabler for the multi-fuel HOPE aircraft. The engines follow a typical GTF engine architecture with a bypass and a core stream. Compression is achieved through a fan, a 3-stage intermediate-pressure compressor (IPC), and a 9-stage high-pressure compressor (HPC). The HPC is connected via a high-pressure spool to the 2-stage high-pressure turbine (HPT). Both the fan and IPC are driven by a 4-stage low-pressure turbine (LPT). In addition, the fan is linked to the low-pressure shaft via a fixed ratio gearbox. To ensure material temperature limits of the HPT and LPT, cooling air is extracted from the HPC. Compared to a conventional GTF architecture, the multi-fuel power plants of the HOPE project feature combustion chambers that can burn 100% SAF, 100% LH_2 or a mixture of the two. The engine architecture of the multi-fuel UHBR engines is depicted in Figure 2.

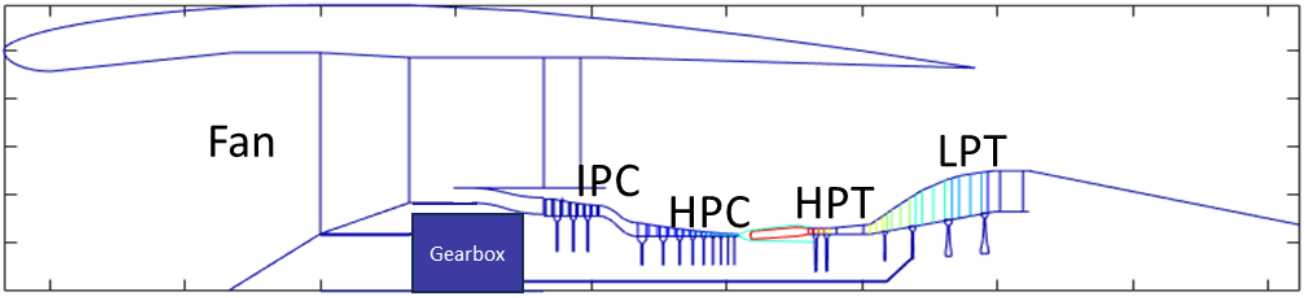


Figure 2: Multi-fuel UHBR GTF engine layout

The performance, dimensions and emissions implications for multi-fuel UHBR GTF engines have already been assessed by Zhao et al. [9] in their in-house aircraft engine simulation framework GESTPAN (GEneral Stationary and Transient Propulsion ANalysis) [10]. Thermodynamic properties for all SAF and H_2 fuel mixtures as well as combustion products were adapted from NASA's Chemical Equilibrium with Applications (CEA) database [11]. Based on the performance calculated in GESTPAN, masses and dimensions of the engine were estimated with the Chalmers in-house model WEICO

(WEIght and COst estimation) [12].

Although initial simulations and experiments indicate a promising outlook for multi-fuel combustors [13, 14], the technology still carries a high level of uncertainty in terms of engine-level integration due to its low technology readiness level. Subsequently, for the present study, the multi-fuel combustion chamber in HOPE is assumed to have no negative impact on the power plant mass. In addition, as the FC-APU provides all power for the all-electric aircraft subsystems, the engines are not required to provide any customer bleed air or electrical power during nominal operation. However, in case the FC-APU is partially or fully inoperative, the multi-fuel power plants are still equipped with back-up generators which can be utilized to bridge insufficient power output of the FC-APU.

To capture all under-wing engine related sensitivities on aircraft-level, feedforward neural network engine surrogate models [15] were created based on the generated results of GESTPAN and WEICO. The implemented engine surrogate models enable the aircraft sizing workflow to update the engine design (i.e., performance, mass and dimensions) based on the required design thrust.

2.3.2 Fuel Cell Auxiliary Power Unit

For the multi-fuel HOPE aircraft presented in this paper, the FC-APU system is based on high-temperature proton exchange membrane fuel cells (HT-PEMFCs). The fuel cell system (FCS) operates at a temperature of 160°C and is designed to be self-sufficient, meaning that it must account for all system-specific power requirements (e.g., coolant pumps or cathode air compressors), as well as the required powers of the aircraft subsystems. The FC-APU system architecture is presented in Figure 3. The system consists of five component domains: the fuel cell stack, the anode stream components, the cathode stream components, the thermal management system (TMS) and the electrical components. The LH_2 tank and fuel supply to the fuel cell are accounted for on the aircraft level analysis separately.

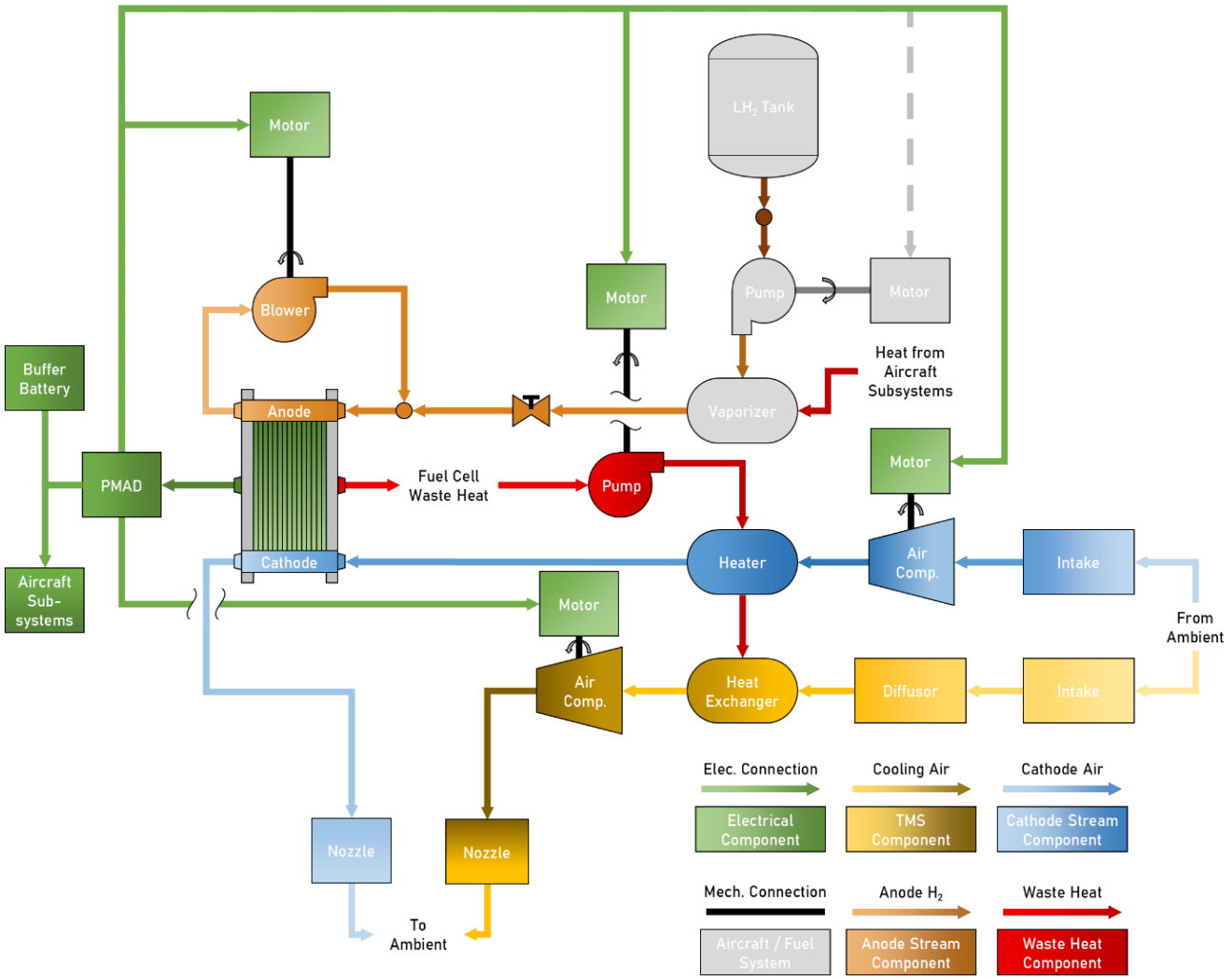


Figure 3: HT-PEMFC FC-APU system architecture

The FCS is modelled using the Bauhaus Luftfahrt in-house tool Hybrid Propulsion Environment (HyPE), which was previously introduced by Kolb et al. [16]. The modelling approach follows a bottom-up principle, starting at the cell level and progressing to the stack and then the complete system level. At the cell level, a pressure and temperature dependent polarization curve modelling is applied (see [17–19]) to assess varying operating conditions throughout the entire aircraft mission. As the assessed FCS represents an EIS date of 2035, it is assumed that future HT-PEMFCs achieve a similar operating characteristic as current low-temperature proton exchange membrane fuel cells (LT-PEMFC). Therefore, the polarization curve behavior of state-of-the-art LT-PEMFCs is applied for this evaluation [16, 20].

The fuel cell (FC) stack is sized to meet the FCS's desired power requirements while staying within a maximum stack voltage or amperage, achieved by connecting the cells in parallel and / or in series. At the system level, the power management and distribution (PMAD) system and electrical machines are accounted for at a low-fidelity level by considering simple electrical efficiencies. The TMS, in this case a ram-air based system, is modelled in the Bauhaus Luftfahrt in-house framework Innovative Cooling Concept Environment (ICCE) and is based on steady-state fluid simulation, allowing for a complete analysis of the TMS power and stream tube drag [21]. The ram-air TMS designed for the FC-APU consists of an intake, a diffusor, a compact heat exchanger, an optional puller fan and a nozzle [16, 21].

For the estimation of mass and volume of the FC stack and electrical components, specific powers and power densities are defined as presented in Table 2. Components such as compressors are estimated based on the approach described by Tornabene et al. [22]. The TMS mass and volume are estimated using the ICCE ram-air heat exchanger sizing routine [21].

Table 2: FCS specific powers and power densities

Parameter	Unit	Value
Stack Specific Power	[kW/kg]	5.0
Stack Power Density	[kW/L]	4.5
Power Electronics Specific Power	[kW/kg]	17.5
Power Electronics Power Density	[kW/L]	20.4
Electric Motor Specific Power	[kW/kg]	19.1
Electric Motor Power Density	[kW/L]	35.1

All effects in terms of FC-APU mass, volume, fuel consumption and drag are accounted for in the aircraft integrated assessment. To be able to integrate the FCS modelling into the aircraft design workflow, the above-mentioned tools and frameworks were used to create feedforward neural network surrogate models [15] to enable varying design and off-design inputs while simultaneously reducing overall calculation runtime.

2.3.3 Aircraft Subsystem Power Estimation

As previously mentioned, the primary role of the FC-APU is to supply the aircraft with electrical power for the aircraft's subsystems. As the multi-fuel aircraft is equipped with an all-electric subsystem architecture, the design power for the FCS is substantially larger than a regular APU. The all-electric aircraft subsystems mission power profile is derived using the approach presented by van Wensveen et al. [23]. Subsystems powers are estimated based on Air Transport Association (ATA) chapters. Smaller power consumers are scaled based on maximum take-off mass (MTOM) or the number of passengers. Larger power consumers such as the environmental control system (ECS, ATA 21), flight controls (ATA 27) and ice & rain protection (ATA 30) are estimated based on approaches by Chakraborty [24], Rao [25] and Meier et al. [26], respectively. In addition, the FC-APU must account for under-wing engine relight scenarios. The electrical power required for relighting is derived from the starting power of the General Electric GEnx take-off power for the Boeing 787 [27] and scaled to maximum engine thrust. As the aircraft has two distinct energy carriers on board, the FC-APU also must also provide the necessary power for the LH_2 fuel system, which is set to a constant demand of 140 kW according to an initial first-guess estimation. This is the total electrical power required to transport the LH_2 from the tank to the engines and FC-APU. The full aircraft subsystems power mission power profile for the design mission (3000 nmi) is presented in Figure 4.

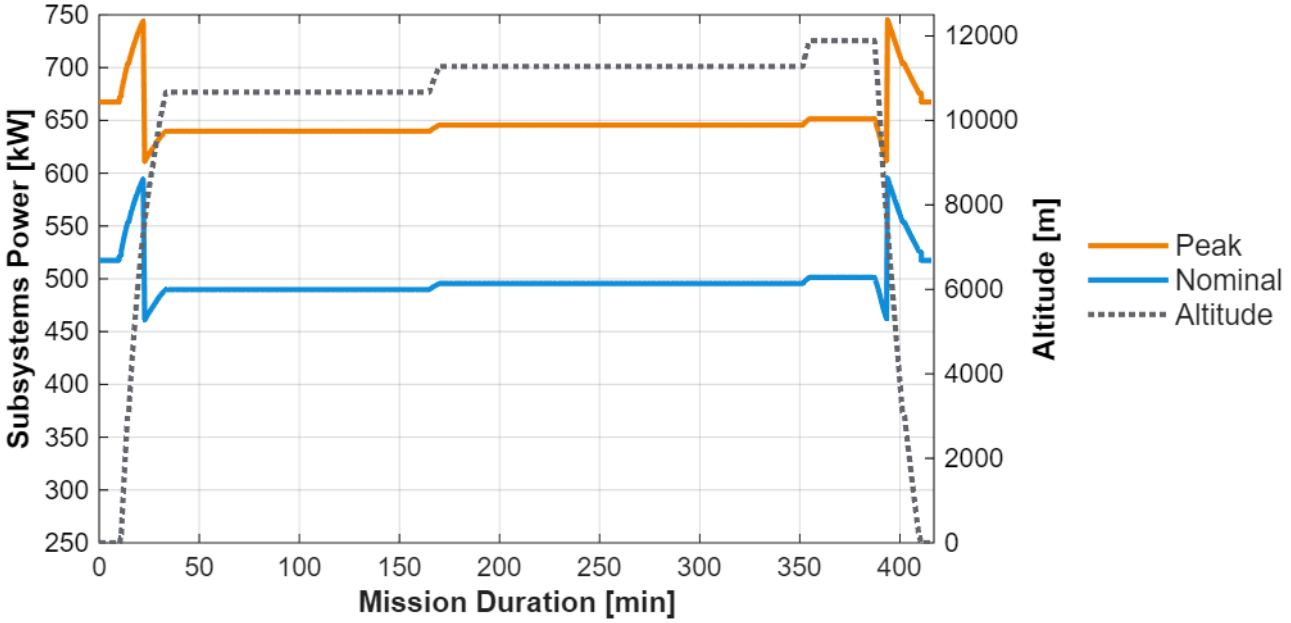


Figure 4: Multi-fuel aircraft subsystems mission power profile

As the capability to re-light an engine is crucial for all mission points, two aircraft subsystem power curves can be obtained. The peak power curve (orange) represents all aircraft subsystem powers including the engine relight scenario. It provides the design requirements for the FC-APU system. The FC-APU system is sized in such a way that all mission segment power demands of the peak power curve can be fulfilled. Subsequently, the highest output power (i.e., design power) falls into the climb segment at 25000 ft. In this point, the ice & rain protection is still turned on, while the power demand of the ECS is already significantly increased. The nominal power curve (blue) represents the typical subsystems power demand, reaching just under 500 kW during nominal cruise.

2.4 Aircraft Sizing Strategy

This study was conducted using the Bauhaus Luftfahrt Aircraft Design Environment (BLADE) [8], which is developed in-house for conducting overall aircraft design activities and the evaluation of new technologies on the overall aircraft level. It consists of discipline- and component-based calculation modules, which are executed sequentially in an aircraft design workflow.

BLADE contains an extensive set of methods to conduct aircraft preliminary design. After specifying the TLARs, mission definitions and the performance requirements, the design process begins with the fuselage design. The fuselage geometry is designed in a way to accommodate the specified number of passengers in the given layout while adhering to regulations. If existing, the LH_2 tank is also sized and considered in the fuselage length determination [28]. After the fuselage design is completed, the wing is sized and positioned using a given wing loading and static margin in the aftmost flyable CG position. The available fuel volume inside the wing is also calculated at this stage. The empennage is sized using volume coefficients or area ratios, depending on which input results in the larger tailplane. Each tailplane is positioned using a given gap to the fuselage end from the trailing edge. In the case of the T-tail, the vertical tailplane (VTP) is positioned using this gap definition, and the HTP root leading edge is placed at the VTP tip leading edge. Engine design and performance estimation is undertaken next, using the previously mentioned feedforward neural networks to determine the engine mass, dimensions and performance characteristics. The aerodynamic characteristics of the whole aircraft are determined using methods based on Torenbeek [29], in both low- and high-speed regimes. This includes a trimming routine alongside a wave drag estimation method based on Malone & Mason [30]. The landing gear is sized next, using a predetermined position and evaluating multiple safety angles, such as the tail strike, longitudinal and lateral stability and bank safety angles [31, 32] to yield a minimum required length. Aircraft subsystems masses are then estimated using FLOPS methods [33] and the overall aircraft design masses are computed. As the last calculation routine, the performance estimation module is executed, which sequentially solves the aircraft equations of motion for a discretized set of mission points, with the aircraft being modeled as a point mass. These modules are executed sequentially until convergence is reached and all performance targets are satisfied. After each run of the workflow, certain design parameters, such as the engine design thrust or wing area can be automatically adapted to meet specified design requirements or performance targets, requiring

minimal intervention from the user.

Some BLADE modules need to be enhanced with methods specific to multi-fuel aircraft design and performance estimation in off-design conditions. As mentioned in Section 2.3, the multi-fuel engine deck is integrated into BLADE using feedforward neural networks. Since the center-of-gravity (CG) position of the whole aircraft is of utmost importance for the estimation of trim drag in a multi-fuel configuration due to the large lever arm of LH_2 storage, the performance estimation module is enhanced with the capability of storing the amount of fuel on board for each fuel type at each mission point. This information is used to calculate the CG at each mission point, enabling the calculation of trim drag from the aerodynamic polars, which are sensitive to the CG location. The LH_2 tank design tool of BLADE is capable of conducting the thermomechanical design of aluminum pressure vessels isolated with closed-cell polyurethane foam. However, this choice of materials is not satisfactory, since a metallic tank would be significantly heavier than a composite tank [34] and the thermal performance of the isolation material would yield to large isolation thicknesses. Therefore, material properties of a carbon-fiber reinforced polymer (CFRP) laminate under cryogenic conditions [35] are used to size the tank structure with a safety factor of 2. A modified version of the Lockheed equation [36] is implemented to enable the estimation of thermal properties of multi-layer insulation (MLI). The number of MLI layers is iterated to achieve the target boil-off rate for the tank sizing. A liner is used to prevent hydrogen permeation. The LH_2 fuel system for this study includes the cryogenic fuel lines from the tank to the engines and the FC-APU, alongside the required pumps and valves to transport the fuel in a liquid state. The mass of this system is not calculated on the component level, it is set to 650 kg as a target for the envisaged EIS, in coordination with industry experts on the advisory board of the project.

A central question when designing this multi-fuel aircraft is determining the LH_2 tank size. With a larger tank, the multi-fuel aircraft becomes more similar to a solely LH_2-powered aircraft, incurring more performance penalties as the fuselage and LH_2 tank grow larger. Therefore, the LH_2 tank must be sized as small as possible, while being able to serve as many of the routes as possible using LH_2 only as trip fuel. These requirements conflict with each other and a good compromise must be found. For this purpose, an analysis of the global SMR aircraft network is conducted using real-world flight scheduling data for 2024 [37]. In this analysis, the total number of available seat miles (ASM) and the number of flights are grouped for mission block distance. These parameters are then cumulatively summed over increasing distance and divided by the total sum of each value to determine the share of flights or ASM for each block distance. The resulting graph is illustrated in Figure 5.

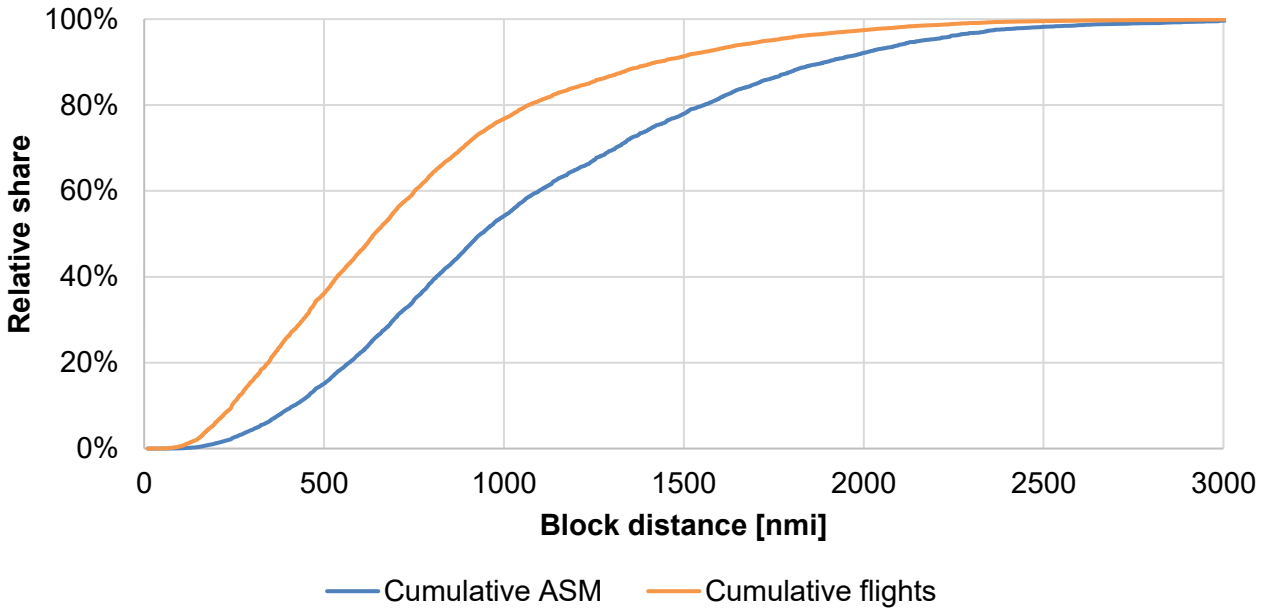


Figure 5: Share of ASM and flights over block distance for the global SMR network

The increase in number of cumulative flights over the block distance is steeper than the increase in the cumulative ASM. Around 1000 nmi, the rate of increase in number of flights with increasing block distance starts to diminish, with a value of approximately 80% of all scheduled flights having less than 1000 nmi as the block distance. At the same point, approximately 55% of all scheduled ASM can be fulfilled. Since the block distance linearly affects the ASM, shorter flights have a smaller impact on the

ASM than longer flights. To further understand this effect, the distribution of ASM and number of flights over the block distance is analyzed as the next step by grouping flights into 100 nmi blocks and summing up the number of flights and ASM. The results of this analysis are shown in Figure 6.

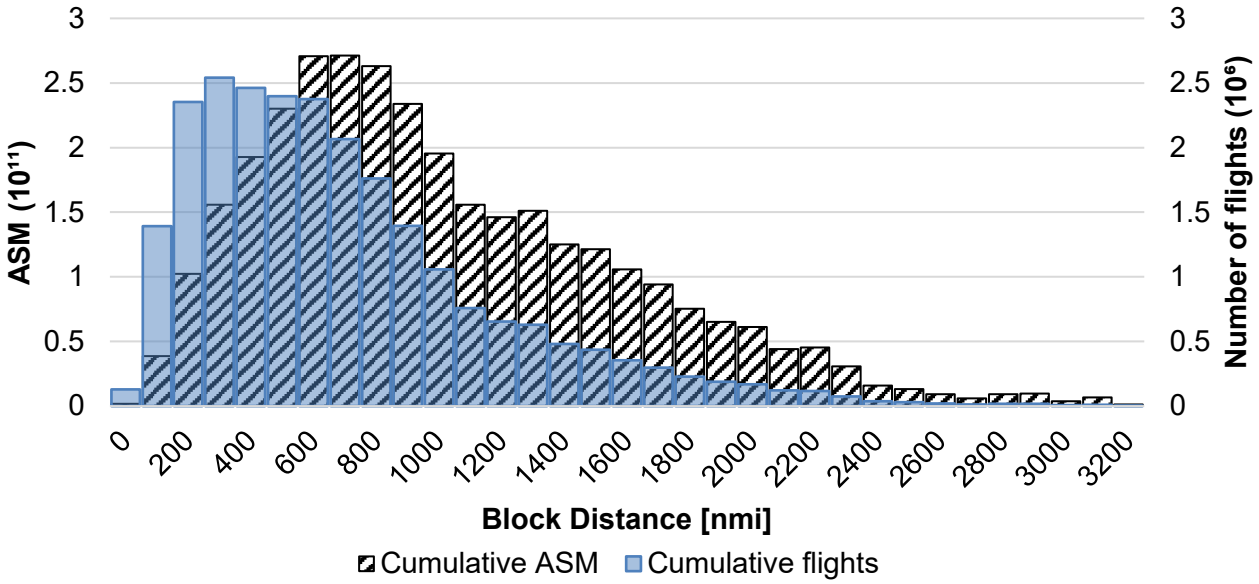


Figure 6: ASM and number of flights over discrete block distances

It can be seen from the analysis that short flights have a much higher frequency than longer flights and the peak of the ASM values is at a higher block distance than the peak in number of flights. Nevertheless, both peaks can be flown by an aircraft which can fly a block distance of 1000 nmi using LH_2 only. Because of these reasons, the LH_2 tank is sized for a mission with 1000 nmi block distance. The strategy on how to use the LH_2 capacity in the design mission is critical to how the aircraft is sized. Requiring the aircraft to fulfill the design range without using any LH_2 would be conservative and lead to a less efficient design, since the LH_2 fuel storage and distribution systems are included in the airframe but are not used in the sizing mission. Additionally, the FC-APU requires LH_2 to function, and the aircraft subsystems are powered by the FC-APU, rendering LH_2 essential for nominal operations. Therefore, the resulting amount of LH_2, which is required for a mission with 1000 nmi of block distance, is used completely during the design mission. The most energy-efficient way of utilizing both fuels during the design mission would be to burn the heavy kerosene/SAF first to enable the aircraft to be as light as possible during the mission. However, this would require a certain redundancy in the LH_2 storage system in case of a tank failure, since there would be no alternative energy carrier on board if a failure was to occur after the hydrocarbon fuel is depleted. To avoid this redundancy requirement, various segments of the design mission are assigned different fuel consumption strategies. An illustration describing this strategy is shown in Figure 7.

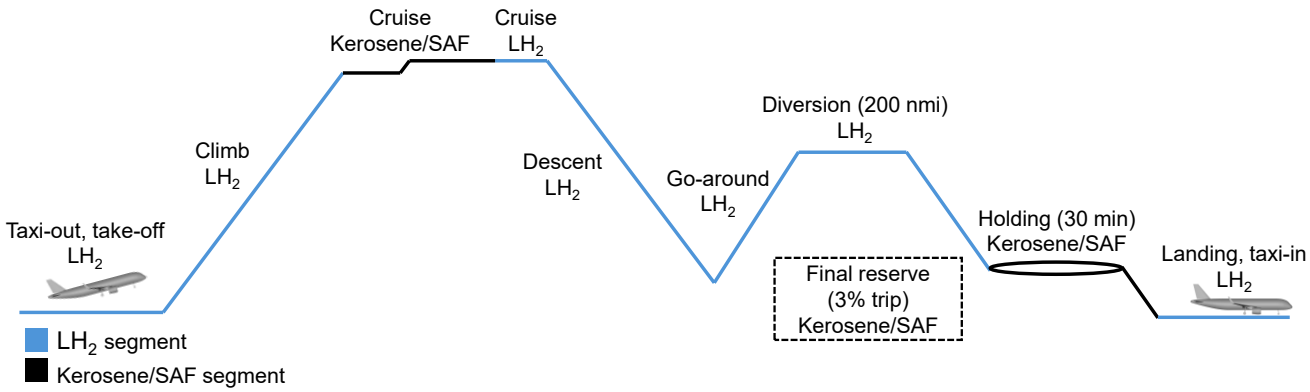


Figure 7: Energy carrier utilization strategy during the design mission for multi-fuel aircraft

From the beginning of the mission until the initial climb, LH_2 is used as fuel. The reason behind this is twofold: to keep the local emissions to a minimum at the landing & take-off (LTO) cycle and lower altitudes, as well as the increased maximum rated thrust from the engines under LH_2 operation. This

allows a smaller engine to satisfy all aircraft-level performance requirements in the design mission, since more rated thrust is available when using LH_2 as fuel, compared to kerosene/SAF. Further explanation regarding the rated thrust characteristic of the multi-fuel engine is provided in Section 3.4. As soon as top-of-climb is reached, the aircraft starts burning kerosene/SAF to get as light as possible, as early as possible during the mission. A switch to LH_2 occurs during cruise, when only enough kerosene/SAF is left on board to fulfill the final reserve and holding segments. The rest of the reserve mission is flown on LH_2. This strategy ensures that both fuels are not depleted until the aircraft reaches the end of the mission. In off-design missions under 1000 nmi, the block distance is flown completely using LH_2 and the reserves are flown using kerosene/SAF to maximize LH_2 utilization. For larger distances, additional kerosene/SAF is burned at the beginning of the cruise phase to achieve the required range. In all missions, enough LH_2 to keep the FC-APU running at each mission point is carried, even if the segment itself is flown using kerosene/SAF only.

3. Results and Discussion

In this chapter, the resulting multi-fuel aircraft are compared to the kerosene-fueled HOPE-BL. First the geometries are compared, followed by the aircraft masses and aerodynamics. The multi-fuel propulsion system results are then presented, comparing the engine design and off-design characteristics. The synthesis of these results is then presented in the form of field and mission performance characteristics. For all tables shown in this chapter, the delta values show relative changes to the HOPE-BL.

3.1 Geometries

A geometric comparison in terms of a 3-view is shown in Figure 8. Additionally, relevant geometric data are listed in Table 3.

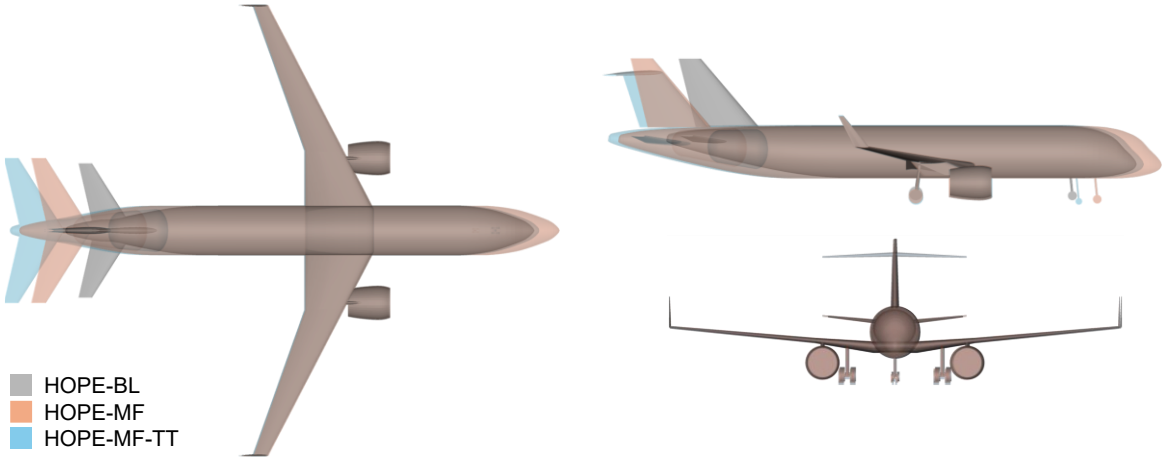


Figure 8: Geometric comparison of all aircraft

Table 3: Geometric data

Parameter	Unit	HOPE-BL	HOPE-MF	Δ	HOPE-MF-TT	Δ
Wing area	[m²]	107.9	107.7	-0.2%	108.0	0.1%
Wingspan	[m]	36	36	0.0%	36	0.0%
Wing aspect ratio	[-]	12	12	0.0%	12	0.0%
Wing loading	[kg/m²]	650	670	3.1%	658	1.2%
Fuselage length	[m]	37.57	43.26	15.1%	42.26	12.5%
Landing gear length	[m]	2.33	2.44	4.7%	2.54	9.0%

The fuselage length increase for the multi-fuel concepts is apparent. Nevertheless, the multi-fuel T-tail configuration exhibits a smaller fuselage length increase compared to the conventional configuration. The placement of the HTP on top of the VTP frees up space in the rear fuselage, which enables the LH_2 tank to move further aft and reduce the fuselage length. The wing size stays relatively constant. The reason for this is that the 36 m span constraint and the maximum aspect ratio of 12, which is defined in the project requirements, effectively dictate the wing area. With a smaller wing, the aspect ratio would increase to higher values while keeping the same span. A larger wing with the same aspect ratio would then be larger than the 36 m span constraint, requiring the removal of winglets and the usage of folding wingtips. With an aspect ratio limit of 12, the wing size would have to increase

considerably to yield a large enough span increase to compensate for the removal of winglets. However, such a large wing is significantly heavier than a smaller wing with winglets. Therefore, the winglets and the span constraint are retained.

Concerning the HOPE-BL wing geometric parameters, there are small differences regarding the wing area and aspect ratio compared to [8]. This is rooted in the change of the wing reference area definition, which included a swept leading edge inside the fuselage, yielding a slightly larger area with the same exposed wing planform.

3.2 Masses

In this section, the overall aircraft masses are compared between the three aircraft. Table 4 shows the relevant values. A more detailed mass breakdown is provided in the appendix.

Table 4: Mass data

Parameter	Unit	HOPE-BL	HOPE-MF	Δ	HOPE-MF-TT	Δ
Fuselage	[kg]	8458	9404	11.2%	9189	8.6%
HTP	[kg]	455	526	15.6%	524	15.1%
VTP	[kg]	438	429	-2.1%	505	15.3%
Systems	[kg]	5185	5577	7.6%	5529	6.6%
LH_2 fuel system	[kg]	0	650	n/a	650	n/a
LH_2 tank	[kg]	0	663	n/a	760	n/a
Operating empty mass	[kg]	38787	42470	9.5%	41877	8.0%
Maximum take-off mass	[kg]	69990	72178	3.1%	71070	1.5%

As expected, the HOPE-BL exhibits the lowest overall aircraft masses, since it has no additional LH_2 storage and distribution system and a shorter fuselage. The increase in fuselage mass is lower for the HOPE-MF-TT in comparison to the HOPE-MF, mirroring the geometric results. While the HTP masses for both multi-fuel aircraft are very similar, the VTP mass of the HOPE-MF-TT is increased considerably due to the additional structural reinforcements which are required in a T-tail configuration. Both multi-fuel aircraft feature the same assumed LH_2 fuel system mass. The LH_2 tank mass, however, exhibits a significant increase from HOPE-MF to HOPE-MF-TT. Further information regarding the tank sizing parameters and the resulting values are introduced next to further explain this result.

As mentioned previously in Section 2.4, a thermomechanical sizing process is conducted for LH_2 tank sizing. While determining the required tank size for a given usable fuel mass, additional considerations must be taken into account, such as the unusable fuel and ullage fraction, which play a role in determining the total volume of the tank. For this study, an unusable fuel fraction of 10% and an ullage fraction of 3% of the usable fuel mass are assumed. A gap of 50.8 cm to the fuselage bottom skin and 25.4 cm in all other directions to the fuselage skin is prescribed for structural integration and crashworthiness considerations. The design maximum internal pressure is set to 2.5 bar and a target boil-off rate of 0.1% per hour is established for the insulation sizing. The results for the HOPE-MF and HOPE-MF-TT tanks are listed in Table 5 below.

Table 5: LH_2 tank characteristics

Parameter	Unit	HOPE-MF	HOPE-MF-TT	Δ
Total volume	[m^3]	30.2	29.6	-1.6%
Usable fuel volume	[m^3]	23.4	22.5	-3.7%
Length	[m]	4.84	5.94	23.0%
Surface area	[m^2]	49.96	52.12	4.3%
Forward diameter	[m]	3.28	3.16	-3.5%
Aft diameter	[m]	3.04	2.65	-4.9%
Total thickness (with insulation)	[m]	0.085	0.089	4.3%
Tank mass	[kg]	663	760	14.7%
Gravimetric index	[-]	0.7	0.66	-5.2%

Even though the total and usable volume of the HOPE-MF-TT tank is smaller, the overall tank mass increases. This increase is also disproportionately high, when compared to the increase in surface area. When looking at the geometric features of both tanks, it becomes apparent that the length-to-

diameter-ratio of the HOPE-MF tank is lower than the HOPE-MF-TT tank, making it closer to a spherical shape, which would be the optimal solution in terms of structural mass for a pressure vessel. The HOPE-MF-TT tank deviates significantly from a spherical form, the change between the forward and aft diameters is larger and the overall tank length is increased, which is shown in Figure 9. This is due to the installation position of the tank inside the fuselage, which is more tapered in the case of the HOPE-MF-TT. These effects result in the reduction of the gravimetric index of the tank by 5.2%.

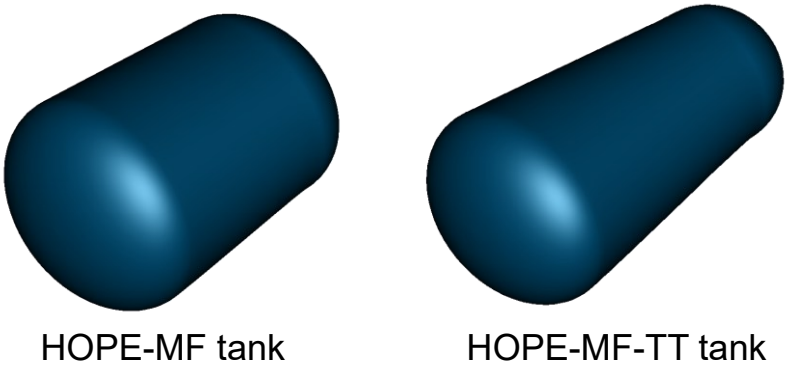


Figure 9: HOPE-MF and HOPE-MF-TT LH_2 tanks

3.3 Aerodynamics

To evaluate the aerodynamic performance of all aircraft, the lift-to-drag ratio (L/D) is analyzed over the lift coefficient (C_L) at the cruising altitude for the typical mission of 1000 nmi for all aircraft. The operating point at mid-cruise is also of interest. An illustration showing both is displayed in Figure 10.

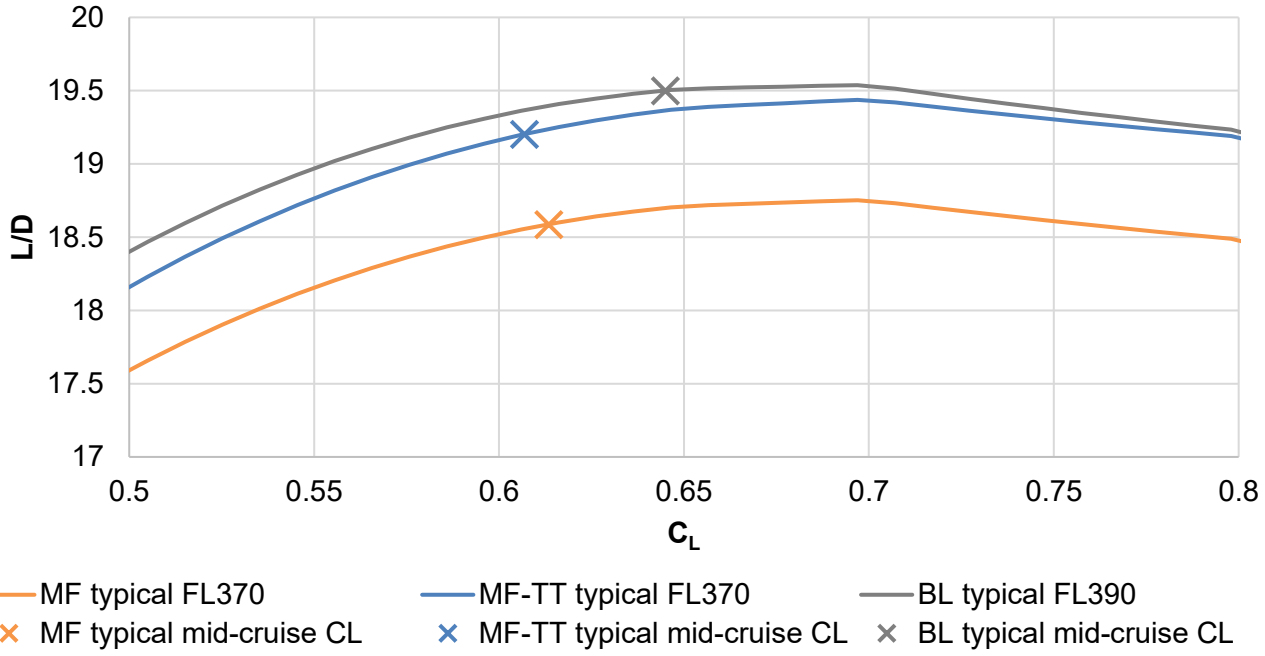


Figure 10: Aerodynamic performance comparison

The HOPE-BL exhibits the highest overall L/D over the entire C_L range for all aircraft, because of its lower zero-lift drag originating from the shorter fuselage. The HOPE-MF has the lowest L/D over the envelope, whereas the HOPE-MF-TT lies in between, matching with the change in fuselage length. The cruise altitude for both multi-fuel aircraft is the same, whereas the HOPE-BL can cruise higher because of its overall lower mass at mid-cruise. The mid-cruise C_L for both multi-fuel aircraft match well with the operating empty masses (OEM) of both aircraft, the HOPE-MF with the higher OEM exhibiting a higher C_L than the HOPE-MF-TT. In general, the operating L/Ds of the HOPE-MF and HOPE-MF-TT are 3.7% and 1.5% lower than the HOPE-BL, respectively.

3.4 Propulsion System and Aircraft Subsystems

The following sections provide an overview of the final designs of the under-wing power plants and FC-APU system integrated into the presented multi-fuel aircraft.

3.4.1 Multi-Fuel Ultra-High Bypass Ratio Turbofan Engines

As described in Section 2.4, the multi-fuel UHBR GTF engines of the multi-fuel HOPE aircraft were iteratively sized in the BLADE aircraft design loop to meet all performance requirements and TLARs. The design point of the engines is set to an artificial top-of-climb (TOC) point at Mach 0.78, 10668 m and an ISA temperature deviation of 10 K. The overall pressure ratio (OPR) of the engines is set to 50 with a design burner exit temperature (T_4) of 1725 K. Although the engines are capable of burning pure hydrogen, their design point is set to 100% SAF operation. The main reason for this design approach is that a 100% LH_2 sized engine would have to run hotter on 100% SAF to maintain the same performance in case the LH_2 tank or fuel system in the aircraft fails (see also Zhao et al. [9]). This would exceed the set temperature limits of the engine, rendering the design insufficient. However, sizing the engine to 100% SAF has the advantage that with 100% LH_2 combustion, more thrust is available. Especially during LTO operations this can be beneficial for faster climb rates and a subsequent reduction in emissions and noise in and around the airport. For LTO the multi-fuel engine running on pure LH_2 achieves around 12% more thrust than with pure SAF. As a result, LTO is always flown on 100% LH_2.

The final engine of the multi-fuel T-tail aircraft has a bare engine mass of 1879 kg. Including the nacelle system and structure, the mass amounts to 2942 kg. Per engine a pylon of 539 kg is required. The engine performance of the conventional tail and T-tail multi-fuel aircraft is very similar. Therefore, only the key engine performance parameters of the T-tail aircraft for TOC, cruise (CR) and take-off (TO) are listed in Table 6. As the FC-APU supplies all aircraft subsystems, the power offtake of the engine is zero.

Table 6: Multi-fuel engine parameters for TOC, CR and TO conditions of the multi-fuel T-tail aircraft

Parameter	Unit	TOC (100% SAF)	CR (100% SAF)	CR (100% LH_2)	TO (100% LH_2)
Mach number	[-]	0.78	0.78	0.78	0.23
Altitude	[m]	10668	10668	10668	0
ISA deviation	[K]	10	0	0	0
Streamtube thrust	[kN]	19.8	17.0	17.0	107.5
Net specific thrust	[m/s]	82.9	71.7	71.7	174.8
Streamtube TSFC	[g/kN/s]	14.0	13.6	4.8	3.2
BPR	[-]	15.5	17.1	17.0	14.6
OPR	[-]	50.0	46.0	46.1	53.4
Inlet mass flow	[kg/s]	239	237	237	615
Compressor exit temperature (T_3)	[K]	854	791	793	977
Burner exit temperature (T_4)	[K]	1725	1570	1524	1900
Power offtake	[kW]	0	0	0	0

To avoid exceeding the aforementioned operating limits of the multi-fuel engines, ratings for take-off and maximum climb were implemented and applied to the aircraft integrated engine performance. Figure 11 shows the ratings for the multi-fuel engines with 100% SAF operation (A) and 100% LH_2 operation (B). It is apparent that full hydrogen operation allows for higher thrust generation before reaching the engine limiters. Although the fuel flow and thrust-specific fuel consumption (TSFC) in 100% LH_2 operation are significantly reduced compared to pure SAF combustion, the thrust specific power consumption (TSPC) stays fairly constant for both maximum climb-rated cases (see Figure 11).

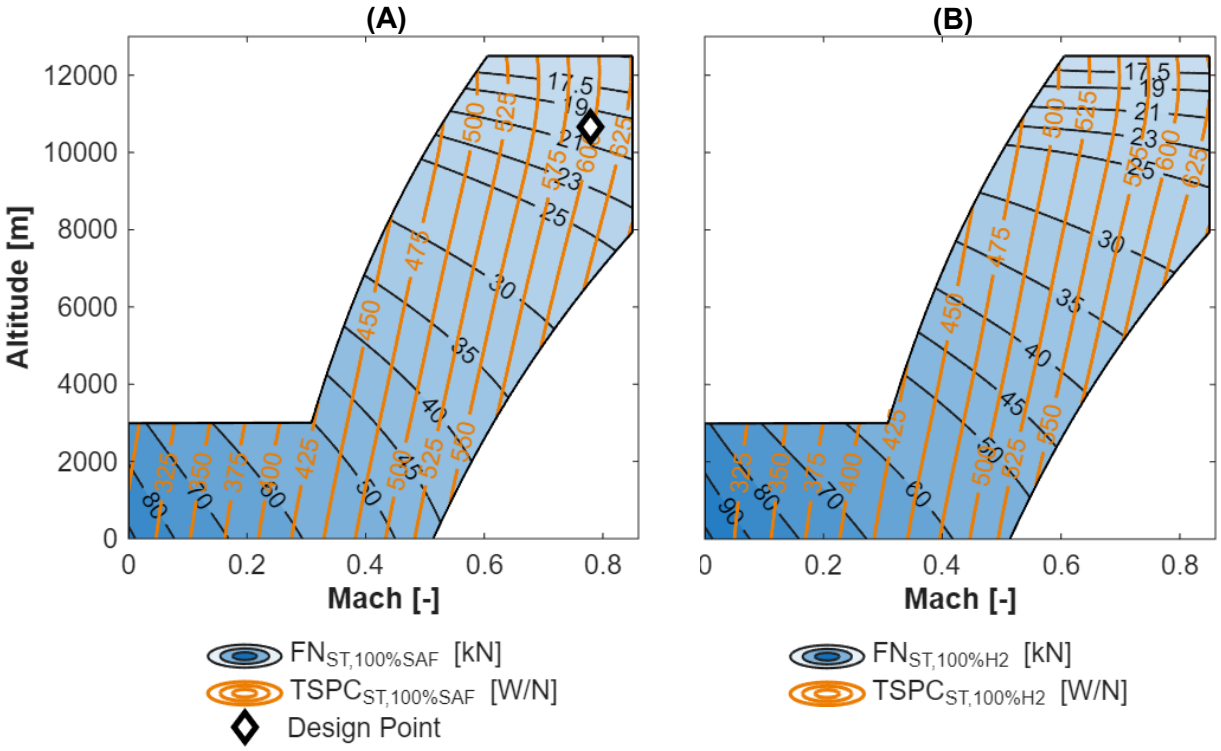


Figure 11: Maximum climb-rated mission envelope for 100% SAF (A) and 100% H_2 (B)

3.4.2 Fuel Cell-Auxiliary Power Unit

Based on the previously defined FCS sizing approach and aircraft subsystems power demands in Sections 2.3.2 and 2.3.3, the FC-APU system is designed and sized to sufficiently fulfill all nominal and peak power demands of the aircraft subsystems. The key operating parameters and design results of the entire FCS are listed in Table 7. The peak power demand of the aircraft subsystems falls into the climb segment (see Figure 4), which is simultaneously the FCS design point. For a typical cruise segment, the FCS consumes 0.0075 kg/s of hydrogen.

Table 7: FC-APU system parameters for design and cruise

Fuel Cell System Parameter	**Unit**	**Value**
Design Mach Number	[-]	0.72
Design Altitude	[m]	7620
Design ISA Deviation	[K]	10
Design Fuel Cell Operating Temperature	[°C]	160
Design Fuel Cell Operating Pressure	[atm]	1.0
Fuel Cell Operating Pressure Range	[atm]	1.0 – 3.0
Design Output Power (incl. Engine Relight)	[kW]	745
Cruise Output Power	[kW]	489
Fuel Cell System Mass	[kg]	360
Design Fuel Cell System Specific Power	[kW/kg]	2.07
Cruise Fuel Cell System Specific Power	[kW/kg]	1.36
Design Fuel Cell System Power Density	[kW/L]	0.94
Cruise Fuel Cell System Power Density	[kW/L]	0.62
Design Fuel Cell Stack Efficiency	[%]	60.0
Design Fuel Cell System Efficiency	[%]	51.1
Cruise Fuel Cell Stack Efficiency	[%]	62.8
Cruise Fuel Cell System Efficiency	[%]	54.0
Cruise Thermal Management System Heat	[kW]	282
Cruise Fuel Cell System Drag	[N]	31.5

The FC-APU is integrated into the aircraft in the aft of the fuselage, replacing the conventional APU system. The mass of the FC-APU system amounts to 360 kg with the FC stack contributing 48.1% of the total mass. The balance-of-plant (BoP) accounts for 25.5% of the system mass, including a buffer battery which is sized to provide the design system power output for 60 seconds. The total volume of the system is calculated to be 0.793 m³.

Figure 12 provides an overview of the FC-APU performance in the block design mission for stack power, BoP power, aircraft subsystems power demand and TMS drag. During nominal cruise operation, the stack provides around 577 kW of which 81 kW are required for powering the BoP components (e.g., compressors, pumps and electrical losses). The highest mission stack power is required during take-off, amounting to 1 MW. In this operating point the BoP requires 478 kW, almost half of the stack power. 150 kW of the BoP power in take-off can be attributed to the puller fan of the of the TMS which is activated during low-speed operations to ensure sufficient air flow through the heat exchangers and correct FC heat dissipation.

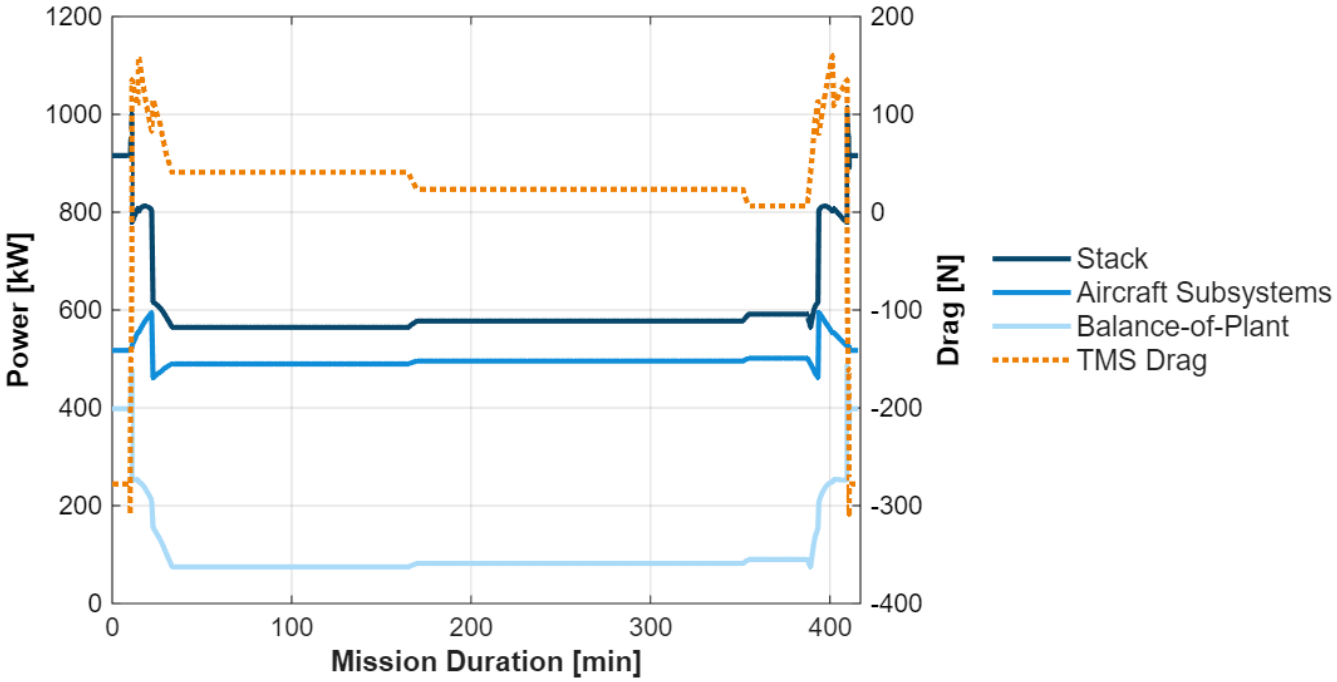


Figure 12: Block design mission FC-APU powers and TMS drag

For the cruise segment, the ram-air TMS system is almost drag neutral reaching between 6 to 40 N of drag depending on the cruise altitude. As the TMS puller fan is active during take-off, the TMS even has a thrust benefit, reaching around 300 N of forward thrust.

3.5 Performance

Some key performance characteristics for all three aircraft are shown in Table 8.

Table 8: Point, field and mission performance comparison

Parameter	Unit	HOPE-BL	HOPE-MF	Δ	HOPE-MF-TT	Δ
Engine design thrust	[kN]	19.8	20.8	5.1%	19.8	0.0%
Take-off field length (MTOM, SL, ISA)	[m]	1935	1695	-12.4%	1719	-11.2%
Landing field length (MLM, SL, ISA)	[m]	1320	1324	0.3%	1317	-0.2%
Vref (MLM, SL, ISA)	[kts]	128	132	3.4%	131	2.7%
Time-to-climb	[min]	28.2	21.6	-23.4%	22.4	-20.4%
Top-of-climb SEP	[fpm]	346	526	52.0%	515	49.0%
OEI ceiling SEP (FL170, ISA+10)	[fpm]	300	300	0.0%	300	0.0%
Initial climb altitude	[ft]	35000	35000	0.0%	35000	0.0%
Design mission block energy	[MJ]	488984	531661	8.7%	508276	3.9%
Typical mission block energy	[MJ]	166122	180862	8.9%	173773	4.6%

The design thrust of the HOPE-BL and HOPE-MF-TT are the same, whereas the HOPE-MF has a slightly larger engine because of the higher mass and worse aerodynamics. Both multi-fuel aircraft exhibit significantly improved take-off performance because of the higher rated thrust under LH_2 operation. The same trend is also exhibited in the climb performance metrics, where both multi-fuel aircraft outperform the HOPE-BL. The most restrictive performance metric for engine sizing is the OEI ceiling specific excess power (SEP) for all aircraft. When comparing the energy consumption, the HOPE-BL is the most efficient, owing to its lower empty mass and better aerodynamic characteristics. When comparing the HOPE-MF to the HOPE-MF-TT, it can be seen that the aircraft-level penalty of the multi-fuel propulsion system can be approximately halved with a more efficient use of LH_2 tank integration space.

In addition to comparing specific missions, it is also important to analyze the entire available operational envelope of all aircraft to evaluate the flexibility of each concept. A suitable way of showing operational flexibility is with the payload-range diagram, which is illustrated in Figure 13 for all aircraft.

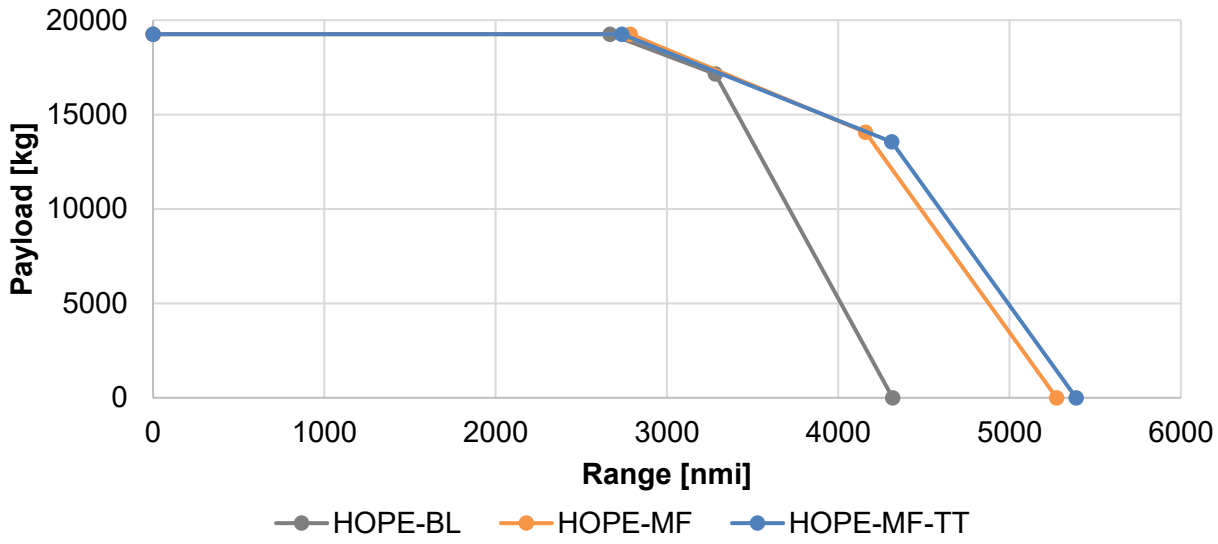


Figure 13: Payload-range diagram

All aircraft exhibit a similar maximum range while flying at the maximum structural payload. When compared to the HOPE-BL, both multi-fuel aircraft exhibit a significantly larger trade between payload and range. The additional energy storage capacity in the form of the LH_2 tank enables this larger trade. This additional range capability would allow the multi-fuel aircraft to fly transatlantic missions with a significantly increased payload, making them operationally more capable than a comparable kerosene-only design.

To evaluate the fuel costs of operating the multi-fuel aircraft against the HOPE-BL, fuel cost estimates for Jet-A, hydroprocessed esters and fatty acids (HEFA), electro-SAF (eSAF) and LH_2 have been compiled from previous research [38, 39], which are used to derive an average fuel price in the future according to ReFuelEU regulations [40]. The resulting fuel prices are shown in Table 9, whereas the resulting fuel costs in 2040 and 2050 for the HOPE-BL and HOPE-MF-TT corresponding to the design and typical missions are shown in Table 10.

Table 9: Energy carrier cost until 2050 [38, 39]

Energy Carrier	Unit	2035	2040	2045	2050
Jet-A	[US$/MWh]	76.65	82.45	85.42	85.56
HEFA	[US$/MWh]	106.54	101.97	97.30	92.54
eSAF (EU)	[US$/MWh]	267.30	242.55	225.15	215.11
LH_2	[US$/MWh]	109.77	100.02	95.85	94.07

Table 10: Fuel cost for HOPE-BL and HOPE-MF-TT

Year	Unit	BL Des.	BL Typ.	MF-TT Des.	MF-TT Typ.	Δ Des.	Δ Typ.
2040	[US$]	14070	4780	14492	4826	3.00%	0.97%
2050	[US$]	18190	6179	17454	4539	-4.05%	-26.54%

The energy costs for HEFA, eSAF and LH_2 continuously go down from 2035 until 2050, whereas Jet-A costs increase in the same period. At the same time, the shares of HEFA and eSAF in the fuel mix increase, in accordance with the ReFuelEU regulations, making the hydrocarbon-based operations more expensive. For 2040, the HOPE-MF-TT exhibits a slight penalty in fuel costs for both missions. However, in 2050, the typical mission fuel costs are significantly lower than the HOPE-BL due to the 100% LH_2 utilization. A slight advantage is achieved in the design mission as well, but the magnitude is much lower, since the HOPE-MF-TT is energetically less efficient and the relative share of LH_2 to hydrocarbon fuel is significantly lower, compared to the typical mission.

4. Conclusion and Outlook

In this paper, the methodology for designing a multi-fuel SMR aircraft is described. The TLARs are introduced, along with the aircraft derivation strategy and the multi-fuel powerplant characteristics. The reasoning behind the design point for the LH_2 tank is described, followed by the LH_2 utilization strategy in design and off-design conditions. The results show that the integration of the multi-fuel propulsion system increases the fuselage length and the OEM, while decreasing aerodynamic efficiency of the aircraft in cruise conditions. However, the utilization of LH_2 increases the maximum rated thrust of the engines, enabling an engine with a similar design thrust as for the HOPE-BL to be able to power the multi-fuel aircraft. A more efficient structural integration of the LH_2 tank has advantages regarding fuselage length, OEM and aerodynamic performance. This can be achieved using a T-tail configuration, which allows a more efficient usage of the tail cone space for the LH_2 tank. The synthesis of these effects yields a higher energy consumption of 8.9% concerning the typical mission for the multi-fuel aircraft in comparison to the HOPE-BL, whereas this penalty is only approximately half as much (4.6%) for the T-tail variant compared to the conventional tail variant. When energy costs tied to the aircraft operation are considered, the multi-fuel aircraft can be beneficial under the ReFuelEU regulation and forecast energy costs, yielding a benefit of approximately 27% in the year 2050 for the typical mission.

5. Contact Author Email Address

For all inquiries, please contact barlas.tuerkyilmaz@bauhaus-luftfahrt.net.

6. Acknowledgments

The authors would like to wholeheartedly thank Adnan Muslić regarding his help with the global SMR fleet analysis.

7. Copyright Statement

The authors confirm that they, and/or their company or organization, hold copyright on all of the original material included in this paper. The authors also confirm that they have obtained permission, from the copyright holder of any third party material included in this paper, to publish it as part of their paper. The authors confirm that they give permission, or have obtained permission from the copyright holder of this paper, for the publication and distribution of this paper as part of the ICAS proceedings or as individual off-prints from the proceedings.

8. Funding Notice

This project has been co-funded by the European Union under the Horizon Europe Research and Innovation program Grant Agreement no. 101096275 and UK Research and Innovation (UKRI) under the UK government's Horizon Europe funding guarantee n° 10068673. Views and opinions expressed are however those of the author(s) only and do not necessarily reflect those of the European Union or the granting authority. Neither the European Union nor the granting authority can be held responsible for them.

9. Abbreviations

APU	Auxiliary power unit
ASM	Available seat mile
ATA	Air Transport Association
BLADE	Bauhaus Luftfahrt Aircraft Design Environment
BLI	Boundary-layer-ingesting
BoP	Balance-of-plant
CEA	Chemical Equilibrium with Applications
CFRP	Carbon-fiber reinforced polymer
CG	Center of gravity
CL	Lift coefficient
CR	Cruise
ECS	Environmental control system
EIS	Entry into service
eSAF	Electro sustainable aviation fuel
FC	Fuel cell
FC-APPU	Fuel-cell auxiliary propulsion and power unit
FC-APU	Fuel-cell auxiliary propulsion unit
FCS	Fuel cell system
FLOPS	Flight Optimization System
GESTPAN	General Stationary and Transient Propulsion Analysis
GTF	Geared turbofan
HEFA	Hydroprocessed esters and fatty acids
HOPE	Hydrogen optimized multi-fuel propulsion system for clean and silent aircraft
HPC	High pressure compressor
HPT	High pressure turbine
HTP	Horizontal tailplane
HTP	Horizontal tailplane
HT-PEMFC	High-temperature proton exchange membrane fuel cell
HyPE	Hybrid Propulsion Environment
ICAO	International Civil Aviation Organization
IPC	Intermediate pressure compressor
ISA	International Standard Atmosphere
KCAS	Knots calibrated airspeed
L/D	Lift-to-drag ratio
LFL	Landing field length
LH2	Liquid hydrogen
LPT	Low pressure turbine
LTO	Landing and take-off
LT-PEMFC	Low-temperature proton exchange membrane fuel cell
MLI	Multi-layer insulation
MTOM	Maximum take-off mass
NASA	National Aeronautics and Space Administration
OPR	Overall pressure ratio
PMAD	Power management and distribution
SAF	Sustainable aviation fuel
SEP	Specific excess power
SMR	Short-to-medium-range
T4	Design burner exit temperature
TLAR	Top-level aircraft requirement
TMS	Thermal management system
TO	Take-off
TOC	Top-of-climb
TOFL	Take-off field length
TSFC	Thrust-specific fuel consumption
TSPC	Thrust-specific power consumption
UHBR	Ultra-high bypass ratio
VTP	Vertical tailplane
WEICO	Weight and cost estimation

10. References

1. International Civil Aviation Organization (ICAO): Strategic Plan 2026-2050. https://www.icao.int/sites/default/files/2025-02/ICAO-Strategic-Plan-2026-2050-V2_0.pdf. Accessed 20 April 2026
2. Lee, D.S., Fahey, D.W., Skowron, A., Allen, M.R., Burkhardt, U., Chen, Q., Doherty, S.J., Freeman, S., Forster, P.M., Fuglestvedt, J., Gettelman, A., León, R.R. de, Lim, L.L., Lund, M.T., Millar, R.J., Owen, B., Penner, J.E., Pitari, G., Prather, M.J., Sausen, R., Wilcox, L.J.: The contribution of global aviation to anthropogenic climate forcing for 2000 to 2018. Atmospheric environment (Oxford, England : 1994) (2021). https://doi.org/10.1016/j.atmosenv.2020.117834
3. Trudell, J.: Dual Hydrogen-Jet Fuel Aircraft. A path to low carbon emissions. Energy & Mobility Technology, Systems and Value Chain Conference & Expo, Cleveland, Ohio, 12 September 2023
4. Rischmüller, U.C.J., Lessis, A., Egerer, P., Hornung, M.: Conceptual Design of a Hydrogen-Hybrid Dual-Fuel Regional Aircraft Retrofit. Aerospace (2024).

https://doi.org/10.3390/aerospace11020123
5. Rüd, K., Scholz, D.: Lower risk approach for low emission passenger aircraft : combined LH2 and kerosene propulsion (2025)
6. Esposito, M., Nugnes, V., Silberhorn, D., Marco, A. de, Zill, T.: Design of Dual-Fuel Aircraft Concepts: A Potential Intermediate Step in the Transition towards Hydrogen-Powered Aviation (2025)
7. European Commission: Hydrogen Optimized multi-fuel Propulsion system for clean and silEnt aircraft, Grant agreement ID: 101096275. https://doi.org/10.3030/101096275
8. Türkyilmaz, B., Lüdemann, M., Kolb, M.G., Lessis, A.: Design of a Short-To-Medium-Range Baseline Aircraft with an Entry into Service in 2035 for the HOPE Project. Aerospace (2025). https://doi.org/10.3390/aerospace12070585
9. Zhao, X., Grönstedt, T., Kolb, M.G.: Assessment of multi-fuel powered turbofans: Performance, dimensions and emissions. Chinese Journal of Aeronautics (2026). https://doi.org/10.1016/j.cja.2026.104082
10. Grönstedt, T.: Development of methods for analysis and optimization of complex jet engine systems. Zugl.: Göteborg, Chalmers Univ., Diss., 2000. Doktorsavhandlingar vid Chalmers Tekniska Högskola, N.S., 1595. Chalmers Univ. of Technology, Göteborg (2000)
11. Gordon, S., Mcbride, B.J.: Computer program for calculation of complex chemical equilibrium compositions and applications. Part 1: Analysis
12. Grönstedt, T., Au, D., Kyprianidis, K., Ogaji, S.: Low-Pressure System Component Advancements and Its Influence on Future Turbofan Engine Emissions. In: Proceedings of the ASME Turbo Expo 2009, Orlando, Florida, USA, June 8-12, pp. 505–516 (2009)
13. Palanti, L., Mazzei, L., Bianchini, C., Link, S., Dave, K., Domenico, F. de, Rao, A.G.: CFD-Based Scouting for the Design of a Multi-Fuel Kerosene/Hydrogen Atmospheric Burner. In: The 34th Congress of the International Council of the Aeronautical Sciences, Florence, Italy, 9 - 3 September (2024)
14. Dave, K., Link, S., Domenico, F. de, Schrijer, F., Scarano, F., Gangoli Rao, A.: Kerosene-H2 blending effects on flame properties in a multi-fuel combustor. Fuel Communications (2025). https://doi.org/10.1016/j.jfueco.2025.100139
15. Seitz, A.: Advanced Methods for Propulsion System Integration in Aircraft Conceptual Design. Dissertation, TUM (Technische Universität München). https://mediatum.ub.tum.de/doc/1079430/1079430.pdf (2012)
16. Kolb, M.G., Seitz, A., Türkyilmaz, B., Ma, Y., Hornung, M.: Modelling and Initial Assessment of a Fuel Cell Auxiliary Propulsion and Power Unit. In: The 34th Congress of the International Council of the Aeronautical Sciences, Florence, Italy, 9 - 3 September (2024)
17. Larminie, J., Dicks, A.: Fuel Cell Systems Explained. John Wiley & Sons, West Sussex, England (2003)
18. Newman, J., Balsara, N.P.: Electrochemical systems. The Electrochemical Society series. Wiley, Hoboken, NJ (2021)
19. Spiegel, C.: PEM Fuel Cell Modeling and Simulation Using Matlab. ELSEVIER (2008)
20. EH Group: EH Fuel Cell Stacks. Product data sheet 2023-A (2023)
21. Kellermann, H.: Design of Thermal Management Systems for Future Aircraft. Dissertation, TUM (Technische Universität München) (2023)
22. Tornabene, R., Wang, X., Steffen, C.J., Freeh, J.E.: Development of Parametric Mass and Volume Models for an Aerospace SOFC/Gas Turbine Hybrid System. NASA/TM-2005-213819. NASA (The National Aeronautics and Space Administration); U.S. ARL (United States Army Research Laboratory), Cleveland. https://ntrs.nasa.gov/search.jsp?R=2005020384 (2005). Accessed 11 June 2019
23. van Wensveen, J., Peter, F., Rau, T., Hornung, M.: Assessment of a Fuel Cell Powered Full Electric Subsystem Architecture for the Avacon Research Baseline Aircraft. In: 68. Deutscher Luft- und Raumfahrtkongress (DLRK). 68. Deutscher Luft- und Raumfahrtkongress (DLRK), Darmstadt, Germany, September 30 - October 2 (2019). https://doi.org/10.25967/490114
24. Chakraborty, I.: Subsystem architecture sizing and analysis for aircraft conceptual design. Dissertation, Georgia Institute of Technology. hdl.handle.net/1853/54427 (2015)
25. Rao, N.K.: Influence of Parametric Modelling of Wing Subsystems on the Aircraft Design and Performance. Master's dissertation, TU Delft (Delft University of Technology). http://resolver.tudelft.nl/uuid:a63515a7-0d5f-4038-ba27-5b6279aa1e11 (2017)
26. Meier, O., Scholz, D.: A handbook method for the estimation of power requirements for electrical

de-icing systems. In: DGLR (Deutsche Gesellschaft für Luft- und Raumfahrt) (ed.) 59. Deutscher Luft- und Raumfahrtkongress (DLRK), Hamburg, Germany, August 31 - September 2, 2010 (2010)
27. Daly, M.: IHS Jane's Aero-Engines. IHS Global, Coulsdon, Surrey (2014)
28. Engelmann, M., Hornung, M.: Geometric optimization of hydrogen aircraft fuselages in preliminary design. In: The 34th Congress of the International Council of the Aeronautical Sciences, Florence, Italy, 9 - 3 September (2024)
29. Torenbeek, E.: Synthesis of Subsonic Airplane Design. An introduction to the preliminary design of subsonic general aviation and transport aircraft, with emphasis on layout, aerodynamic design, propulsion and performance. Springer Netherlands, Dordrecht (1982)
30. Malone, B., Mason, W.H.: Multidisciplinary optimization in aircraft design using analytic technology models. Journal of Aircraft (1995). https://doi.org/10.2514/3.46734
31. Currey, N.S.: Aircraft landing gear design. Principles and practices, 4th edn. AIAA education series. AIAA (The American Institute of Aeronautics and Astronautics), Washington, DC (1988)
32. Scholz, D.: Aircraft Design Lecture Notes. Landing Gear Conceptual Design and Integration. https://www.fzt.haw-hamburg.de/pers/Scholz/HOOU/AircraftDesign_12_LandingGear.pdf. Accessed 21 January 2026
33. Wells, D.P., Horvath, B.L., McCullers, L.A.: The Flight Optimization System Weights Estimation Method, NASA/TM–2017–219627/Volume I. NASA (The National Aeronautics and Space Administration), Langley Research Center, Hampton, Virginia, USA. https://ntrs.nasa.gov/citations/20170005851 (2017)
34. Freund, S., Rickert, C., Ravi, V.: Assessment and Optimization of CFRP Liquid Hydrogen Tanks. In: Silberhorn, D. (ed.) Architecting Future Aviation. DLR (2025)
35. Abumeri, G., Kosareo, D., Roche, J.: Cryogenic Composite Tank Design for Next Generation Launch Technology. In: 40th AIAA/ASME/SAE/ASEE Joint Propulsion Conference and Exhibit. 40th AIAA/ASME/SAE/ASEE Joint Propulsion Conference and Exhibit, Fort Lauderdale, Florida. American Institute of Aeronautics and Astronautics, Reston, Virigina (2004). https://doi.org/10.2514/6.2004-3390
36. Hastings, L.J., Hedayat, A., Brown, T.M.: Analytical Modeling and Test Correlation of Variable Density Multilayer Insulation for Cryogenic Storage. NASA/TM-2004-213175. National Aeronautics and Space Administration (2004)
37. OAG (Official Aviation Guide of the Airways): Scheduled flight data 2024 (2024)
38. Zhou, Y., Searle, S., Pavlenko, N.: Current and future cost of e-kerosene in the United States and Europe. International Council on Clean Transportation (ICCT) Working Paper 2022-14 (2022)
39. Dray, L.M., Schäfer, A.W., Grobler, C., Falter, C., Allroggen, F., Stettler, M.E.J., Barrett, S.R.H.: Cost and emissions pathways towards net-zero climate impacts in aviation. Nat. Clim. Chang. (2022). https://doi.org/10.1038/s41558-022-01485-4
40. European Commission: Regulation (EU) 2023/2405 of the European Parliament and of the Council of 18 October 2023 on ensuring a level playing field for sustainable air transport (ReFuelEU Aviation) (Text with EEA relevance). Document 32023R2405. http://data.europa.eu/eli/reg/2023/2405/oj (2023). Accessed 25 March 2025

Appendix

Table A1: Detailed mass breakdown

Parameter	Unit	HOPE-BL	HOPE-MF	Δ	HOPE-MF-TT	Δ
Fuselage	[kg]	8458	9404	11.2%	9189	8.6%
Wings	[kg]	7666	7904	3.1%	7825	2.1%
HTP	[kg]	455	526	15.6%	524	15.1%
VTP	[kg]	438	429	-2.1%	505	15.3%
Landing gear	[kg]	2122	2330	9.8%	2281	7.5%
Engines	[kg]	5881	6214	5.7%	5885	0.1%
Pylons	[kg]	1079	1112	3.1%	1078	-0.1%
Systems	[kg]	5185	5577	7.6%	5529	6.6%
LH_2 fuel system	[kg]	0	650	n/a	650	n/a
LH_2 tank	[kg]	0	663	n/a	760	n/a
Furnishings	[kg]	3058	3058	0.0%	3058	0.0%
Operator's items	[kg]	4446	4446	0.0%	4446	0.0%
Operating empty mass	[kg]	38787	42470	9.5%	41877	8.0%
Payload	[kg]	18000	18000	0.0%	18000	0.0%
Maximum take-off mass	[kg]	69990	72178	3.1%	71070	1.5%
Maximum landing mass	[kg]	60191	63290	5.1%	62635	4.1%